J Membrane Biol (2008) 221:123–132
DOI 10.1007/s00232-007-9084-2

An Outwardly Rectifying and Deactivating Chloride Channel Expressed by Interstitial Cells of Cajal from the Murine Small Intestine

Sean P. Parsons · Kenton M. Sanders

Received: 22 May 2007 / Accepted: 25 October 2007 / Published online: 14 February 2008

Abstract Recent studies have suggested a role for a chloride current in the modulation of pacemaker potentials generated by interstitial cells of Cajal. Patch-clamp recordings were made from inside–out patches of cultured interstitial cells of Cajal from the murine small intestine. The majority of patches were quiescent immediately after excision, but in some patches currents activated spontaneously after a period of 10 min to 1 h. Currents could also be activated by strongly polarizing the patch. It was found that the currents activated in both cases included a chloride channel. This channel could also be activated by ATP and the catalytic subunit of protein kinase A. The channel had conductance states (±SD) of 53 ± 25.35, 126 ± 21.44, 180 ± 12.57 and 211 ± 8.86 pS. It was outwardly rectifying (as a function of open probability) and deactivated (i.e., gave a tail current) but showed no inactivation. The permeability sequence of the channel was $I^- >> Br^- \geq Cl^- > Asp^-$. It was unaffected in magnitude or rectification by changing the free Ca^{2+} concentration of the bath between <10 nM, 100 nM (control) and 2 mM.

Keywords Chloride channel · Interstitial cell of Cajal · Pacemaker potential · Protein kinase A · Tail current · Deactivation · Rectification subconductance

S. P. Parsons · K. M. Sanders
Department of Physiology and Cell Biology, University of Nevada School of Medicine, Reno, NV 89557, UK

S. P. Parsons (✉)
5 Tankerville Road, London SW17 5LL, UK
e-mail: parsons_llabh@yahoo.co.uk

Introduction

In the gastrointestinal (GI) tract, rhythmic motility is driven by a network of specialized cells, called interstitial cells of Cajal (ICC). Histologically, there are two types of ICC: those in the myenteric plexus between circular and longitudinal smooth muscle layers (myenteric ICC) and those dispersed within the smooth muscle itself (intramuscular ICC). Myenteric ICC autonomously and rhythmically depolarize, generating a pacemaker or driving potential (Hirst et al., 2002; Hirst & Edwards, 2001). GI smooth muscle cells have a nonregenerative (graded) response to depolarization. Therefore, the pacemaker potential would be expected to decay exponentially from the plexus. However, both intramuscular and myenteric ICC do depolarize in a regenerative (nongraded) manner in response to depolarization (Hirst et al., 2002). It is this regenerative potential which allows the pacing depolarization to spread throughout the muscle (the "slow wave"), causing smooth muscle contraction via activation of voltage-dependent calcium channels.

The mechanisms of both the pacemaker and regenerative potential are thought to involve inositol trisphosphate–dependent intracellular calcium release and a calcium-dependent (activated or inhibited) ion channel(s) (*see* Koh et al., 2002, for review). A study by Kito & Suzuki (2003) of the murine small intestine has shown that the depolarization and plateau phases of the pacemaker potential are modulated by different currents. $NiCl_2$ decreased the rate of depolarization, suggesting a cationic current is responsible for this primary phase. On the other hand, low extracellular Cl^- or 4,4′-diisothiocyanatostilbene-2,2′-disulfonic acid (DIDS) increased the onset and rate of repolarization, reducing the half-width of the pacemaker potential (the plateau) by half, suggestive of modulation by a chloride current. As similar effects were seen with both low bath Ca^{2+} and 1,2-bis(*o*-

aminophenoxy)ethane-*N,N,N',N'*-tetraacetic acid (BAPTA), the authors suggested that this chloride current was calcium-dependent, a conclusion supported by Hirst & Edwards (2001), who saw the same effect with caffeine on pacemaker potentials in the murine gastric antrum.

In this study, we demonstrate a chloride channel expressed by myenteric ICC of small intestine, with biophysical properties apposite with a role modulating the response to pacemaker potential repolarization–namely, a tail current–but with little steady-state current at physiological potentials (outward rectification) and no apparent calcium dependence. We also show that this channel is activated by ATP and protein kinase A (PKA). The possible relevance of this channel to the pacemaker potential mechanism is discussed.

Materials and Methods

Solutions and Drugs

The names of solutions and their contents are given in Table 1. *N*-Methyl-D-glucamine (NMDG) halide solutions were produced by titration of NMDG with the acids of the halides (HCl/HBr/HI) to pH 5.2 (the stoichiometric point of NMDG with strong acids). The catalytic subunit of PKA (cPKA) was from Promega (Madison, WI). All other chemicals and drugs were from either Sigma (St. Louis, MI) or Fisher (Pittsburgh, PA).

Electrophysiology

ICC were isolated from the jejenum of Balb/C mice at 7–15 days of age and cultured for 3–4 days before use (Koh et al., 2002). The standard cell-attached and excised inside–out patch-clamp configurations were used to record single channels expressed by cultured ICC. Myenteric ICC were identified by their triangulate, multiprocess morphology (Kito & Suzuki, 2003). Pipettes typically had tip resistances of 5–10 MΩ. All recordings were performed at room temperature. Cells were always bathed in 4-(2-hydroxyethyl)-1-piperazineethanesulfonic acid (HEPES)-buffered saline (HS) before gigaseal formation. In some experiments, the bath/pipette solution was either symmetrical cesium (HS_{CS}) or symmetrical NMDG (HS_{NMDG}). The junction potential (V_J) between HS and HS_{CS} was calculated as +4.6 m*V*, and that between HS and HS_{NMDG}, -5.4 m*V*. Voltage-clamp protocols were adjusted accordingly where $V_{app} = V_J - V_M$ (V_{app}, applied potential; V_M, patch potential). Currents were amplified with a CV203BU headstage connected to an Axopatch 200B amplifier and digitally recorded with Clampex 9.0 software via a Digidata 1322A A/D converter (all Axon Instruments, Union City, CA). Unless stated otherwise, the digital sampling rate was 5 kHz. The reference electrode consisted of a chlorided silver wire inserted into a glass capillary, pulled at one end and filled with 3 M KCl in 3% (w/v) agar.

Analysis of Data

For all voltage-clamp protocols, averaged control traces (i.e., traces in the absence of channel activation) were subtracted from traces in the presence of channel activity.

Unitary current amplitude (*u*) was calculated first by binning current values (0.1 or 0.2 pA bins) with a program written in IDL (v6.1; Research Systems, Boulder, CO). These data were then plotted in Origin (Microcal Software,

Table 1 Names of solutions and their contents

	Glucose	Na^+	K^+	Cs^+	Ca^{2+}	Free[a] Ca^{2+}	Mg^{2+}	HEDTA	EDTA	EGTA	$NMDG^+$	Cl^-	Asp^-	X^{-b}
HS	10	135	5		2		1.2					146.4		
HS_{CF}	10	135	5									140		
IN_K			140		0.54	100 nM				1		140		
HS_{CS}	10			140	2		1.2					140.4		
IN_{CS}				140	0.54	100 nM				1		11.08	130	
HS_{NMDG}											140	140		
IN_{NMDG}					0.54[c]	100 nM				1	140			140
LC_{NMDG}					0.161[c]	<10 nM			1		140	140		
HC_{NMDG}					0.323[c]	2 μM		1						

All concentrations in millimoles, except where stated. All solutions contained 10 mM HEPES and were adjusted to pH 7.35 with TrizmaBase

HEDTA N-(hydroxyethyl)-ethylenediaminetriacetate

[a] Values calculated with Winmaxc (Bers, Patton & Nuccitelli, 1994) with T = 20°C, ionic strength = 0.14 M. These values were also confirmed with a calcium electrode constructed by D. Goff based on Baudet, Hove-Madsen & Bers (1994)

[b] Either Cl^-, Br^-, I^- or aspartate

[c] $Ca(OH)_2$

Northhampton, MA) to give an all-points histogram, and peaks in the histogram were fitted with gaussian functions (the center of the gaussian giving the unitary current).

The open probability (P_o) was calculated by dividing the mean current (m) at a particular voltage by the unitary current at the same voltage (Colquhoun & Sigworth, 1995).

$$P_o(V) = \frac{m(V)}{u(V)} \pm \sqrt{\left(\frac{\delta_m}{u}\right)^2 + \left(\frac{m.\delta_u}{u^2}\right)^2} \quad (1)$$

where δ_m is the standard error of m and δ_u is the standard error of u.

Chord conductance values in voltage-ramp data were found with an algorithm based on event detection by difference of slopes and regression (to calculate conductance) by the evaluation of eigenvectors (both methods are described by Seul, O'Gorman & Sammon, 2000). Only events with length >50 ms and regression correlation coefficient (R) >0.9 were considered.

Relative anion permeabilities ($P_{y/x}$) were calculated by equimolar substitution of the bath solution. Reversal potentials (E_{rev}) were calculated by algorithm from averaged voltage ramps (usually 12 ramps/anion/cell). Deriving from the Goldman-Hodgkin-Katz voltage equation (with $z = -1$), $P_{y/x}$ can be calculated as follows from the E_{rev} with either bath solution (E^x_{rev} and E^y_{rev}, respectively):

$$P_{y/x} = \exp\left[\left(E^y_{rev} - E^x_{rev}\right).\frac{F}{RT}\right] \pm \sqrt{\left(\left|\frac{\partial P_{y/x}}{\partial E^y_{rev}}\right|.\delta_y\right)^2 + \left(\left|\frac{\partial P_{y/x}}{\partial E^y_{rev}}\right|.\delta_x\right)^2} \quad (2)$$

where

$$\frac{\partial P_{y/x}}{\partial E^y_{rev}} = -\frac{\partial P_{y/x}}{\partial E^x_{rev}} = \exp\left(-E^x_{rev}.\alpha\right) \times \alpha \times \left(\exp E^y_{rev}\right)^{\alpha} \quad (3)$$

where $\alpha = F/RT$, δ_y is the standard error of E^y_{rev} and δ_x is the standard error of E^x_{rev}.

Results

Spontaneous Activation

Most inside–out patches (>95%) were quiescent immediately after excision from ICC, but currents often activated spontaneously within 10–60 min. To determine whether this spontaneous current was carried by anions or cations, a pipette/bath solution combination (HS_{CS}/IN_{CS}) was employed where the equilibrium potential for chloride (E_{Cl}) was set to −65 mV (with aspartate substitution) and that for monovalent cations (E_{cat}) was set to 0 mV. Ten patches were stepped alternately between these potentials with a 2-min dwell time at each potential. In three patches currents were present at both potentials (outward at 0 mV, inward at −65 mV; Fig. 1), in two only at 0 mV (outward) and in one only at −65 mV (inward). In four patches no currents activated spontaneously after 25 min. The currents at 0 mV were definitively identified as anionic in nature (henceforth I_{Cl}). However, as it was further shown that I_{Cl} has a significant permeability to aspartate (*see below*, Fig. 6), identification of inward current at −65 mV as cationic, when I_{Cl} was present at 0 mV, was not definitive.

I_{Cl} was manifest as a clear unitary current with a generally high open probability but with numerous sojourns to subconductance states (Fig. 1b; *see* Fig. 5 for quantitative analysis) and often complete reduction to such states (Fig. 1a; periods at 0 mV subsequent to that marked [B]). In contrast, a clear unitary current level could not be distinguished for currents at −65 mV (in patches with or without I_{Cl} at 0 mV), and channels responsible for these currents displayed brief flickery openings (Fig. 1c).

Activation by Strong Polarization

Early experiments with inside–out patches from ICC suggested that currents could be activated by strong polarization (>100 mV of either polarity). Using the same protocol and solutions as employed above, patches were held at 0 or −65 mV (Fig. 2a). If currents did not activate spontaneously after 8 min, the patch was repeatedly stepped to +120 mV for 10 s, 0 mV for 20 s and −65 mV for 20 s (Fig. 2b; this protocol was used in other experiments below and will be termed "HYP"). After strong polarization, currents were present at both potentials (−65 and 0 mV). These currents had similar characteristics as the I_{Cl} that activated spontaneously in some patches (a unitary current of 6−8 pA with a high open probability).

Activation by PKA and ATP

I_{Cl} could also be activated by ATP and PKA. The patch was held at 0 mV, with the pipette/bath solutions as before (HS_{CS}/IN_{CS}). Four minutes after excision, 1 mM MgATP was added to the bath, and after a further 4 min, this was supplemented with 100 units • ml^{-1} of bovine heart cPKA (Fig. 3). If there was no response to either ATP or PKA after 16 min from the time of excision, the patch was then subjected to the HYP protocol (as above).

Of 24 patches tested, I_{Cl} was activated in three in response to MgATP, in four to cPKA and in three to HYP. The remaining 14 patches were quiescent after 10 repetitions of HYP. In patches where I_{Cl} activated in response to ATP, subsequent addition of cPKA did not affect I_{Cl}. In the

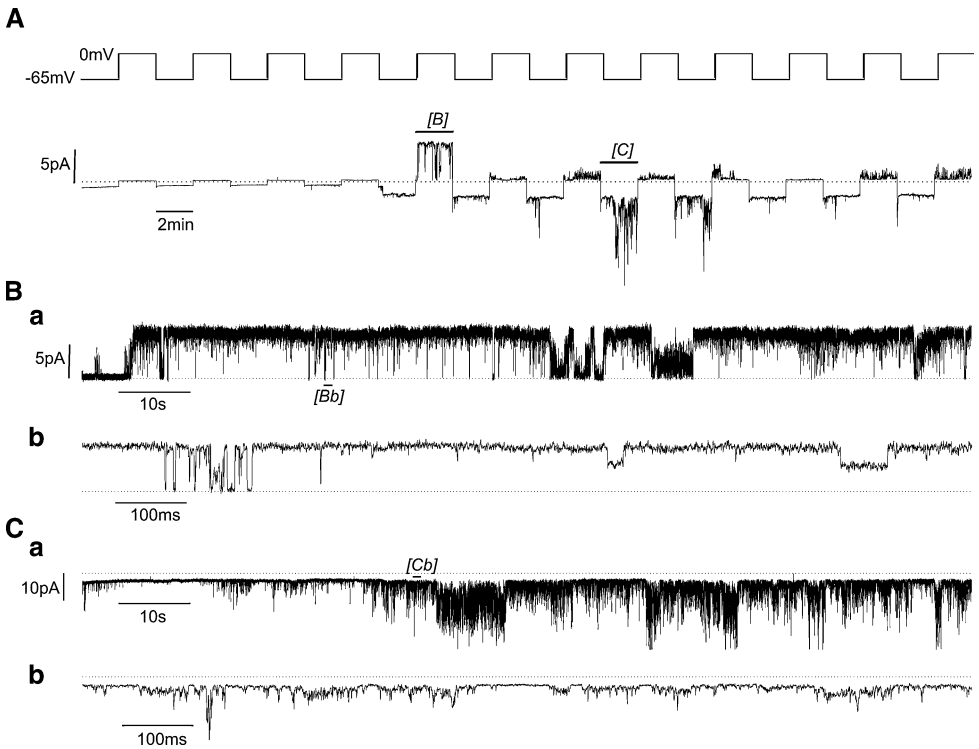

Fig. 1 Spontaneous activation of I_{Cl} and a cationic current in an inside–out patch of an ICC. The pipette solution was HS_{CS} and the bath was IN_{CS}. **a** Beginning immediately after patch excision, the patch was stepped back and forth between −65 m*V* (E_{Cl}) and 0 m*V* (E_{Cs}) for 2 min at each potential (*upper trace* is membrane potential, *lower trace* is corresponding current). The cationic current is the inward current (below the zero current level, *dotted line*) at −65 m*V* and I_{Cl} is the outward current (above the zero current level) at 0 m*V*. The record has been digitally resampled to 10 Hz (from 5 kHz) by adjacent averaging. **b** *a* The fifth 2-min period at 0 m*V* (marked *[B]* in **a**). *b* An expanded 1.2-s period of *a* (marked *[Bb]* in *a*). **c** *a* The eighth 2-min period at −65 m*V* (marked *[C]* in **a**). *b* An expanded 1.2-s period of *a* (marked *[Cb]* in *a*)

seven patches that responded to MgATP or cPKA, there was a delay of >1 min between addition of the stimulants and the onset of activation. This delay was consistent between patches (lower part of Fig. 3), so activation correlated with the addition of the stimulants. The activation times were clustered between ATP and cPKA (332.3 ± 17.3 s for ATP, 676.5 ± 15.3 s for cPKA; $P < 0.00003$ between the two by unpooled *t*-test), as opposed to being randomly distributed as would be expected if activation was spontaneous. Also, by use of the chi-squared test, it was found that the observed distribution of activation times was significantly different from a random distribution (i.e., equal probability for activation during any time period; period = 1 min, $\chi^2 = 27.29$, $P < 0.026$).

Voltage Dependence

The voltage-dependent properties of I_{Cl} were investigated with patches bathed in symmetrical NMDG chloride (HS_{NMDG} in the pipette, IN_{NMDG} in the bath) so that I_{Cl} was isolated at all potentials from cation currents. After activation by either ATP, cPKA (both holding at −50 m*V*) or HYP (in the absence of activation by ATP or PKA), patches were stepped to potentials between −100 and 100 m*V* for 5 s, before returning to −50 m*V* (for 5 s between steps). There was no obvious difference in the behavior or appearance of channels activated by the different methods. Very little current was observed at negative potentials, a stable unitary current was observed at potentials in the range of 20–60 m*V* and a flickery current was observed at potentials >60 m*V* (Fig. 4a, *a*; $n = 22$ runs, 9 patches). There was a clear deactivation of unitary currents after return to −50 m*V* from steps positive to −20 m*V*–i.e., a tail current (Fig. 4a, *a*). These properties (outward rectification and tail current) were seen clearly in averaged traces (Fig. 4a, *b* and *c*).

Unitary currents of I_{Cl} were most stable (unlikely to fluctuate into subconductance states) during the tail current. Therefore, to calculate the unitary conductance of I_{Cl}, patches were held at −50 m*V* before being stepped to +20 m*V* for 4 s and then stepped to potentials between −100 and 100 m*V* for 1 s, to record the unitary tail current (solutions as above, symmetrical NMDG chloride). The unitary current at each potential was then calculated as described in "Materials and Methods." The current–voltage relationship of the unitary tail current was found to be linear through the middle of

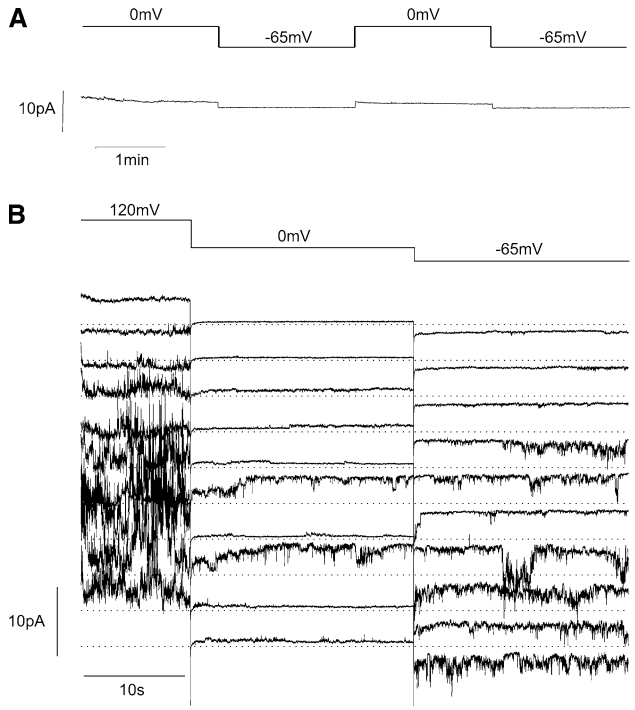

Fig. 2 Activation of I_{Cl} and cationic current by strong polarization. The pipette solution was HS_{CS} and the bath was IN_{CS}. **a** As with Figure 1a, immediately after patch excision the patch was stepped back and forth (twice) between −65 (E_{Cl}) and 0 m*V* (E_{Cs}) for 2 min at each potential. **b** The patch was then advanced repeatedly (10 times) through the following protocol: 120 m*V* for 10 s, 0 m*V* for 20 s and −65 m*V* for 20 s. Subsequent repeats run from top to bottom, with the *dotted lines* indicating the zero current level

the voltage range (Fig. 4b; n = 11 runs, 3 patches), but the slope became more shallow at large potentials (>60, <−60 m*V*), probably indicating saturation of the channel. Fitting of the midrange potentials gave a conductance of ∼190 pS. The voltage/open probability (V/P_o) relationship of I_{Cl} (Fig. 4c) was calculated by dividing the mean step currents (Fig. 4a, *c*, filled circles; n = 22 runs, 9 patches) by the unitary tail currents (Fig. 4b; n = 11 runs, 3 patches) at each voltage. P_o was very low (<0.1) at negative potentials, rising to a peak around +20 m*V* (0.65 ± 0.11) before tailing off to a plateau of ∼0.4 at positive potentials (Fig. 4a, *a*).

Subconductance States

Subconductance states of I_{Cl} were clearly visible in steady-state voltage-clamp records (e.g., Fig. 1b). However, possibly the most efficient method of gaining data about conductance states was through voltage ramps. Patches were held at 0 m*V* and every 12 s stepped to −100 m*V* for 2 s before ramping to +100 m*V* over 2s (100 m*V* • s^{-1}) and then holding at +100 m*V* for a further 2 s. The solutions were HS (pipette) and IN_K (bath). We analyzed 907 such voltage-ramp records from 18 patches (each from a separate cell) quantitatively with an event detection algorithm (*see* "Materials and Methods," Fig. 5a), which detected 2,030 events. The distribution of these events according to chord (slope) conductance (Fig. 5b) showed at least four distinguishable peaks at 53.00, 126.10, 180.76 and 211.36 pS (heights/SDs of 76.67/25.35, 101.37/21.44, 53.51/12.57 and 40.82/8.86, respectively). These were labeled "α," "β," "γ," and "δ," respectively. In addition to these peaks, there were more obscure peaks at >220 and ∼20 pS (labeled "ε").

In addition to chord conductance, the event-detection algorithm recorded the potential midpoint along the line fitted to the event. The codistribution of chord conductance and midpoint potential for all 2,030 events are shown in Figure 5c. The most conspicuous feature of this distribution was the absence of events along an axis of 0 m*V*, except those of ε. Either side of this axis there was a marked asymmetry in the distribution of peaks: at positive potentials α, β, γ, and δ peaks were all equally visible, but at negative potentials the β peak was very dominant (explaining the relative dominance of this peak in Fig. 5b), whereas the α, γ and δ peaks were very obscure.

Permeability and Calcium Dependence

To determine the anion permeability of I_{Cl}, patches were held at 0 m*V* and every 10 s polarized to −80 m*V* for 200 ms before ramping to +80 m*V* over 800 ms. Initially, the patches were bathed in symmetrical NMDG chloride

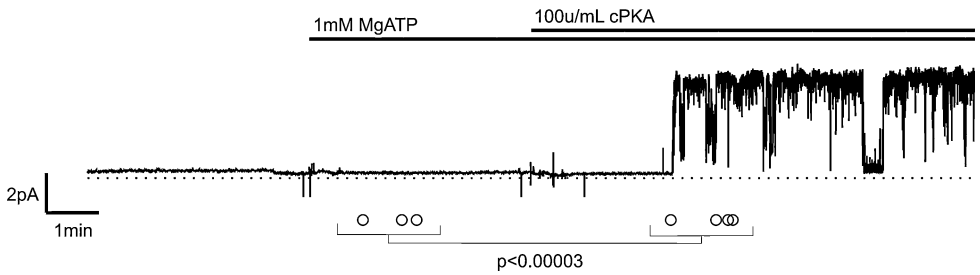

Fig. 3 Activation of I_{Cl} by ATP and PKA. Patches were held at 0 m*V*; the pipette solution was HS_{CS} and the bath was IN_{CS}. MgATP (1 mM) was added to the bath 4 min after patch excision, and this was supplemented by 100 u • ml^{-1} cPKA after a further 4 min. *Circles* below the example current trace indicate the times at which I_{Cl} activated in other patches using the same protocol. The example current trace was resampled to 50 Hz (from 5 kHz)

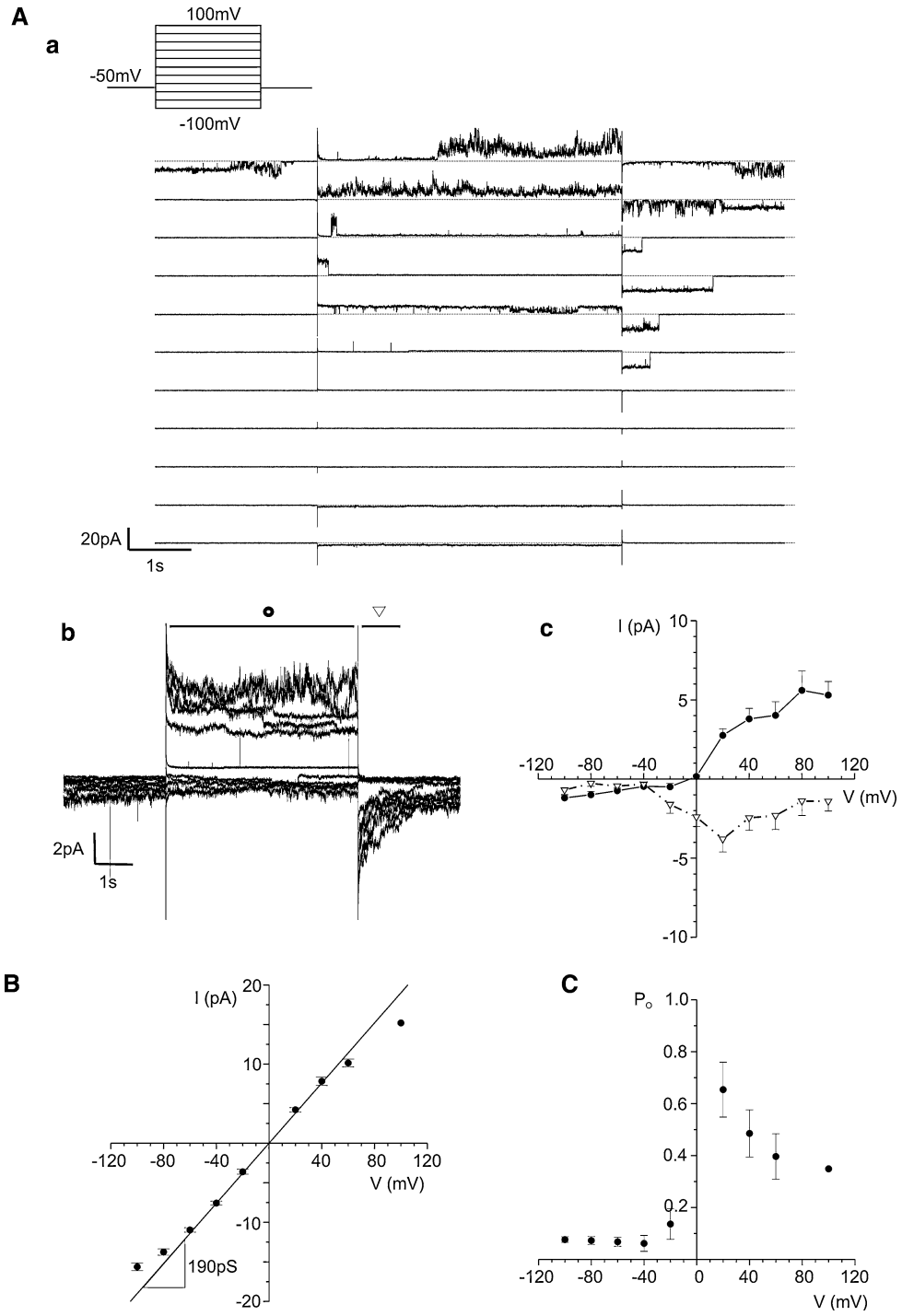

Fig. 4 Voltage dependence of I_{Cl}. **a** Inside–out patches were held at –50 m*V* and stepped to potentials between −100 and 100 m*V* (in 20-m*V* increments) for 5 s before stepping back to −50 m*V*. *a* An example trace from one patch. *b* An averaged trace of 22 runs of the protocol from nine patches. The current values for each sweep were divided by the number of channels in the patch. *c* Current values of *b* averaged over the time periods indicated by the upper bars in *b* (•, step current; ∇, tail current). **b** Unitary tail currents. Inside–out patches were held at −50 m*V*, stepped to +20 m*V* for 4 s and then stepped to potentials between −100 and 100 m*V* (in 20-m*V* increments) for 1 s. Current values from the latter "tail" period were used to construct all-point histograms for each potential, which were fitted with gaussians to calculate unitary currents (*see* "Materials and Methods"). The data were calculated from 11 runs of the protocol from three patches. *n* values for each potential, V(*n*), are −100(6), −80(11), −60(10), −40(11), −20(6), 20(4), 40(4), 60(3), 100(1). The line fitted to the unitary current values (by eye) gives a unitary conductance of 190 pS. **c** Open probability (P_o) was calculated by dividing the step current values (Ac, •) by the unitary tail current values (**b**) at each voltage

(HS_{NMDG} in the pipette, IN_{NMDG} in the bath), before equimolar replacement of the bath chloride with either bromide, iodide or aspartate (Fig. 6). The reversal potentials (E_{rev}) calculated with each anion were then used to calculate the permeability of Br^-, I^- or Asp^- relative to Cl^- ($P_{X/Cl}$, where X is the substitute anion; *see* "Materials and Methods"). E_{rev} for Cl^-, Br^-, I^- and Asp^- were (m*V*) −2.48 ± 0.34, −0.30 ± 0.32, 58.47 ± 3.65 and −41.43 ± 6.82, respectively (n = 5). Therefore, $P_{X/Cl}$ for Br^-, I^- and Asp^- were 1.09 ± 0.02, 11.16 ± 1.62 and 0.21 ± 0.06, respectively (n = 5). The current shifts with each anion (including iodide) were fully reversible, and substitutions were performed in random order. The Cl^-/I^- permeability was also studied on a fractional (vs. equimolar) basis. The fraction of iodide (f_I) is given as $[I^-]/([Cl^-]+[I^-])$. In three patches there was

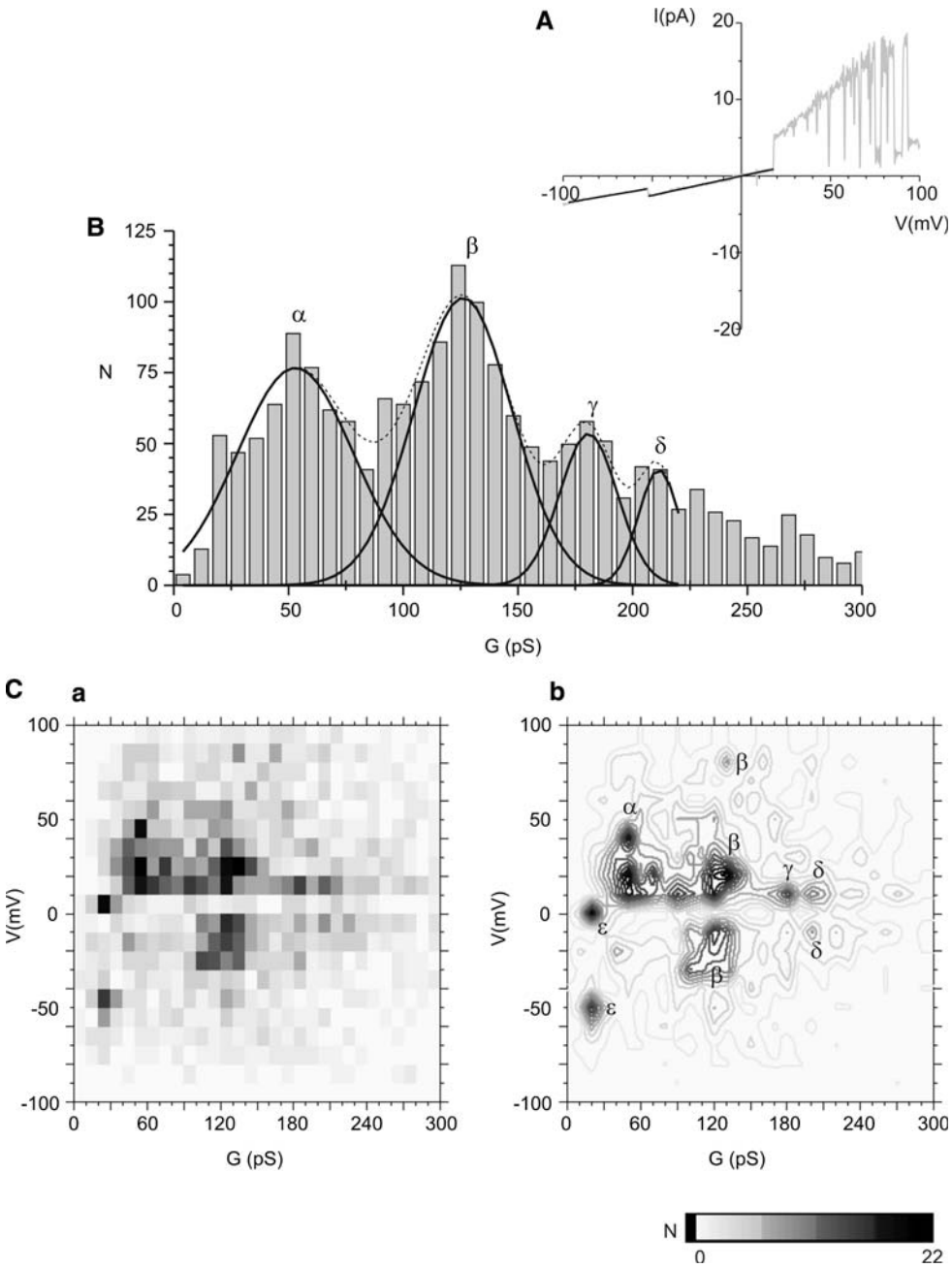

Fig. 5 Subconductance states of I_{Cl}. **a** Example of the operation of the event-detection algorithm on voltage-ramp data. *Gray trace* is the current, and *black lines* are lines fitted to events detected by the algorithm. Note that as the patch was ramped from 100 to −100 m*V*, so time runs from right to left (2 s over the period of the ramp). **b** Distribution of calculated chord/slope conductances. n = 2,030, bin size = 8 pS. *Four black curves* are gaussian functions fitted to the data (mean or center ± SD, 53.00 ± 25.35, 126.10 ± 21.44, 180.76 ± 12.57, 211.36 ± 8.86; left to right). *Black dashed curve* is the sum of these gaussians. **c** Codistribution of event midpoint potential (V) and chord conductance (G). As for **b**, n = 2,030. *a* Two-dimensional histogram with bin size = 10 m*V*/10 pS for midpoint potential/chord conductance, respectively. The n value of each bin is represented by its shading (white = 0 to black = 22, see scale at lower right of **c**). *b* Contour representation of *a* (see "Materials and Methods"). Peaks in the codistribution labeled with Greek letters correspond to peaks in the one-dimensional conductance distribution (**b**)

no significant shift in E_{rev} with f_I = 0.0, 0.05, 0.1 or 0.2 (E_{rev} [m*V*] = −2.62 ± 0.79, −1.84 ± 2.25, −1.08 ± 1.25 and 0.22 ± 1.26, respectively; n = 3). Only at f_I = 0.4 did E_{rev} begin to shift (E_{rev} = 26.83 ± 12.73 m*V*).

To determine the calcium dependence of I_{Cl}, patches (in symmetrical NMDG chloride, as above) were ramped as above. Initially, the free calcium concentration ($[Ca^{2+}]_{free}$) of the bath was 100 nM before replacement with bath solutions, with $[Ca^{2+}]_{free}$ < 10 nM or $[Ca^{2+}]_{free}$ = 2 mM (Fig. 7a). In five patches, changing bath $[Ca^{2+}]_{free}$ had no significant effect on current magnitudes measured at −80 and 80 m*V* (Fig. 7b), with one exception–a small increase in current at −80 m*V* with a change in bath $[Ca^{2+}]_{free}$ from 100 to <10 nM ($P < 0.013$ by paired t-test).

Discussion

Conductance States

In terms of conductance states, the chloride channel described here bears a remarkable resemblance to Cl^- channels described previously by Huizinga et al. (2002) in inside–out patches from cultured ICC of the murine

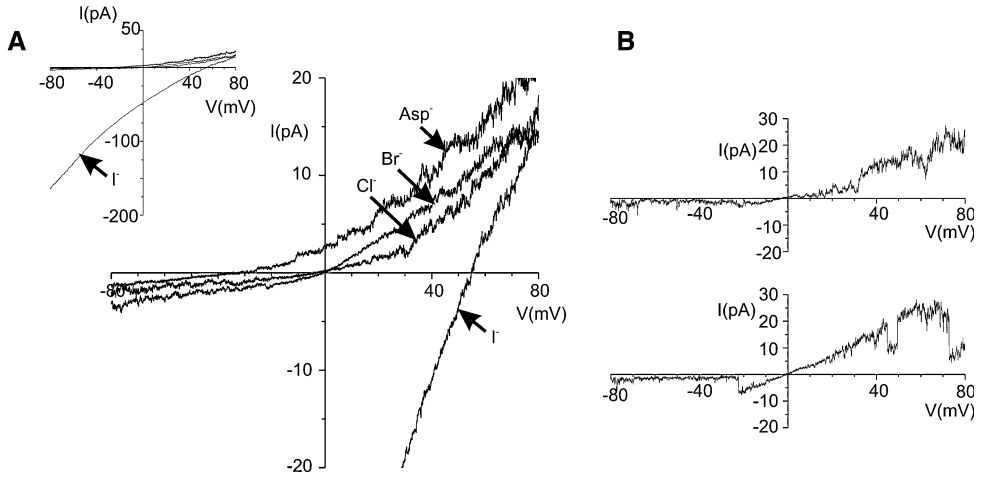

Fig. 6 Permeability of I_{Cl}. **a** Averaged current traces (12 traces per average) for a patch ramped from −80 to 80 m*V* (over 800 ms but shown as a function of voltage) with various bath anions. *Lower right figure* shows the same data as smaller *upper left figure* but with the current axis range reduced. **b** Example traces from the same patch as in **a** (upper in Cl^-, lower in Br^-). The opening of the channel at potentials in the range −30 to 0 m*V* (*lower trace*) was a characteristic feature of many of the sweeps. There are two channels in the patch

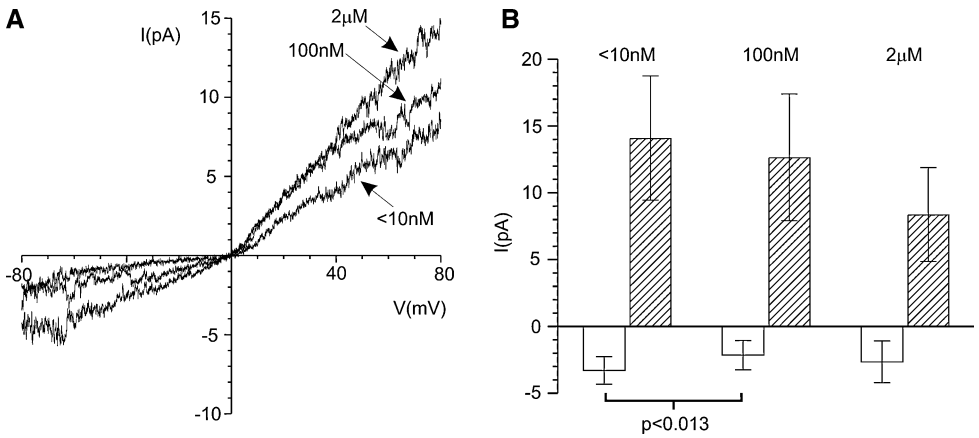

Fig. 7 Calcium independence of I_{Cl}. **a** Averaged current traces (18 traces per average) for a patch ramped from −80 to +80 m*V* (over 800 ms but shown as a function of voltage) with various bath $[Ca^{2+}]_{free}$. **b** Data summarized for five patches (protocol as in **a**). White bars, current at −80 m*V*; hatched bars, current at 80 m*V*. At each potential (−80 or 80 m*V*) paired *t*-tests were performed for $[Ca^{2+}]_{free} < 10$ nM and $[Ca^{2+}]_{free} = 2$ mM, with respect to the values at 100 nM. For only the comparison indicated, $P < 0.05$. Qualitatively similar results were obtained with a steady-state protocol (cf. Fig. 4a)

jejunum (though from CD-1 mice rather than Balb/C). For brevity, the channel we describe here will be termed PACC (PKA- and ATP-activated chloride channel) and the channel described by Huizinga et al. (2002), HCCC (high conductance chloride channel). Analysis of voltage-ramp data by Huizinga et al. (2002) demonstrated three conductance states for HCCC: 62/75, 124/130 and 185/182 pS (Figs. 5, 6). These values are in close correspondence to the $\alpha/\beta/\gamma$ conductances of PACC (mean ± SD = 53 ± 25, 126 ± 21, 180 ± 12 pS), also determined from voltage ramps. It is noticeable that these values are roughly multiples of 60 pS. In addition, we found peaks at 20 pS (ε) and 211 pS (δ). These values are ∼30 pS lower than α or higher than γ, respectively. Thus, the spacing for all the subconductances can be summarized as follows: (ε)30pS(α)60pS(β)60pS(γ)30pS(δ).

ε and δ might be described as "half-subconductances" which bookend the "full subconductances" of α, β and γ. This may represent some symmetry in the ion channel structure/function relationship. ε and δ were not noted by Huizinga et al. (2002) in their ramp data, perhaps because of their small difference from the full conductances. However, they do show a conductance of 217 pS in some steady-state recordings (Fig. 7).

Huizinga et al. (2002) cite similarities between HCCC and the large-conductance chloride channel (LCCC) of rabbit colonic myocytes as characterized by Mayer and colleagues (Sun et al., 1992, 1993). In both inside– and

outside–out patches LCCC had a main unitary conductance of 309 ± 20 pS and four equally spaced subconductances of 60 pS–i.e., the spacing may be summarized as (c_1)60pS(c_2)60pS(c_3)60pS(c_4)60pS(c_{main}). In comparison to the equivalent spacing of PACC, the smallest and largest conductances are now "full" 60 pS, rather than 30 pS.

The 190 pS unitary conductance value obtained from tail current analysis probably reflects an averaging of the γ and δ conductances as the unitary tail current was calculated from an all-points histogram which has less resolution (is more sensitive to noise) than the regression lines used in calculating the subconductances. Nevertheless, the subconductance peaks of PACC do show significant width (standard deviation). To some extent, this may reflect actual variance in the subconductance states or further subconductance states that cannot be resolved (without larger n values). However, much of the width reflects simply the variance introduced by the recording (i.e., instrument noise) and the limitations of the analytic method.

To summarize, ε, α, β and γ are subconductances of δ (the unitary conductance). There is one main reason that ε, α, β, γ and δ are considered conductance levels of a single channel rather than separate channels. In steady-state data (at potentials near 0 m*V*, Fig. 1b) or in tail-current data (Fig. 4a, *a*), the majority of the time the current corresponds to a conductance of 190–200 pS or multiples thereof. In most patches (~60%) this multiple was only ever one (i.e., only one channel), in some (~30%) two (i.e., two channels) and in the rest greater than two (the maximum ever seen was five). In all the patches conductance transitions of <190–200 pS were several orders of magnitude greater in frequency than transitions equal to 190–200 pS, meaning the current record appears as ragged blocks of 190–200 pS conductance (Fig. 1b). Logically then the smaller, more frequent transitions are subconductance transitions.

Rectification

Huizinga et al. (2002) make no mention of rectification. However, in one figure of a voltage-ramp protocol HCCC is outwardly rectifying and in two others it is linear. A linear *I–V* relationship was also observed in a small minority (~5%) of voltage ramps of PACC. In both cases, this linearity is explained by the protocols used. In both cases, patches were held at 0 m*V* and then stepped to a negative potential before ramping to a positive potential. The step from 0 m*V* holding to negative would give rise to a deactivation current at the negative part of the ramp, thus giving the appearance of linearity.

A follow-up report to Huizinga et al. (2002) further characterized HCCC in inside–out patches (Zhu, Mucci & Huizinga, 2005). These authors reported the same conductances as the earlier study. However, they explicitly reported inward rectification for HCCC. There could be one simple explanation for this discrepancy, that the current and voltage values were not inverted for inside–out patch data, to conform with the standard definition of the membrane potential. If a current was outwardly rectifying but this inversion was not carried out, it would appear to rectify inwardly. Similarly, an inwardly rectifying current would appear to rectify outwardly. However, both Huizinga et al. (2002) and Zhu et al. (2005) stated that this inversion was carried out. Therefore, it is curious that these two papers show opposite rectification to one another. Apart from stating that we did invert the current and voltage values in our data, we can provide further support for the outward rectification of PACC. If we were to invert the values again, so that now PACC is inwardly rectifying, we would also invert the permeability sequence of $I^- >> Br^- \geq Cl^- > Asp^-$. Thus, the channel would have a greater permeability to aspartate, an amino acid, than to the much smaller halide ions. For a simple channel, this would seem implausible; and if PACC was some kind of amino acid transporter, then why the huge difference between I^- and the other halides?

Comparison to Other Channels

As mentioned above, Huizinga et al. (2002) remarked on the similarity of HCCC with LCCC in rabbit colonic myocytes (Sun et al., 1992; Sun et al., 1993). There are further properties of LCCC which are reminiscent of PACC: (1) LCCC was quiescent after patch excision but could be induced by strong patch polarization; (2) LCCC was calcium-independent and (3) LCCC had a bell-shaped V/P_o relationship, peaking at 0 m*V*. All of these, apart from the last, are also properties of the "outwardly rectifying chloride channel," or ORCC (*see* Hryciw & Guggino, 2000, for review). As the name suggests, it is outwardly rectifying like PACC (but with a conductance of 90 pS) but it is also activated by PKA and ATP. As with PACC, activation by PKA always requires ATP (as might be expected) but the channel can also be activated by ATP alone. In such cases, it could be that there is some endogenous PKA associated with the patch (perhaps via an anchoring protein such as AKAP). However, there is another interesting possibility. In epithelial cells ORCC is associated with the cystic fibrosis transmembrane receptor (CFTR) chloride channel. ORCC is a member of the ABC transporter family and therefore possesses ATPase activity upon which its activity is dependent. Activation of CFTR in turn activates ORCC in much the same way as the

sulfonyl urea receptor (another ABC member) activates the K_{ATP} channel.

Tail Current and Physiological Function

The PACC gives little steady-state current at physiological resting potentials. However, it does give a tail current which activates with repolarization from potentials depolarized positive to -20 m*V*. Such depolarization would not normally be achieved by the slow wave experienced by the bulk tissue (an amplitude of ~ 30 m*V* from a resting of ~ -70 m*V*; Kito & Suzuki, 2003). However, the pacemaker potentials generated by myenteric ICC are much larger than slow waves (an amplitude of ~ 60 m*V* from a resting of ~ 70 m*V*), so depolarization would reach well within the window for tail current activation. In many types of neuronal cell, inward tail current from a chloride channel generates an "afterdepolarization" following an action potential (Mayer, 1985). By "afterdepolarization" it is meant that repolarization following an action potential is not complete, with the cell remaining for some time (depending on the kinetics of the tail current) a few millivolts depolarized from the final resting potential. This afterdepolarization encourages the generation of further action potentials, leading to a bursting behavior. A study of pacemaker potentials in the guinea pig gastric antrum (Hirst & Edwards, 2002) has shown that roughly a quarter of myenteric ICC generate afterdepolarizations which encourage the generation of "unitary events"–small transient depolarizations of a few millivolts. These unitary events normally occur in the run-up to a pacemaker potential and are thought to be involved in the initiation of regenerative potentials. However, their significance to afterdepolarizations is unknown, and neither is the significance of afterdepolarizations themselves. Interestingly, Hollywood et al. (2003) demonstrated a whole-cell chloride current in rabbit urethral ICC with large tail current and large iodide permeability.

In summary, we conclude that the chloride channel described could be involved in modulating pacemaker afterdepolarization. Further characterization of the tail current will need to be performed, particularly under whole-cell conditions, and the calcium dependence of the channel will need to be resolved. However, the novel and identifying channel characteristics illustrated in this study will greatly help in this–namely, outward rectification, a very large iodide permeability (which could also be useful in whole-tissue studies), a complex set of subconductance states and activation by PKA and ATP.

Acknowledgments This study was supported by a program project grant (P01 DK41315) from the NIDDK of the National Institutes of Health.

References

Baudet S, Hove-Madsen L, Bers DM (1994) How to make and use calcium-specific mini- and microelectrodes. Methods Cell Biol 40:93–113

Bers DM, Patton CW, Nuccitelli R (1994) A practical guide to the preparation of calcium buffers. Methods Cell Biol 40:3–29

Colquhoun D, Sigworth FJ (1995) Fitting and statistical analysis of single-channel records. In: Sakmann B, Neher E (eds) Single-channel recording. Plenum Press, New York, pp 483–587

Hirst GDS, Edwards FR (2001) Generation of slow waves in the antral region of guinea-pig stomach–a stochastic process. J Physiol 535:165–180

Hirst GDS, Bramich NJ, Teramoto N, Suzuki H, Edwards FR (2002) Regenerative component of slow waves in the guinea-pig gastric antrum involves a delayed increase in $[Ca^{2+}]_i$ and Cl^- channels. J Physiol 540:907–919

Hollywood MA, Sergeant GP, McHale NG, Thornbury KD (2003) Activation of a Ca^{2+}-activated Cl^- current by depolarizing steps in rabbit urethral interstitial cells. Am J Physiol 285:C327–C333

Hryciw DH, Guggino WB (2000) Cystic fibrosis transmembrane conductance regulator and the outwardly rectifying chloride channel: a relationship between two chloride channels expressed in epithelial cells. Clin Exp Pharmacol Physiol 27:892–895

Huizinga JD, Zhu Y, Ye J, Molleman A (2002) High conductance chloride channels generate pacemaker currents in interstitial cells of Cajal. Gastroenterology 123:1627–1636

Kito Y, Suzuki H (2003) Properties of pacemaker potentials recorded from myenteric interstitial cells of Cajal distributed in the mouse small intestine. J Physiol 553:803–818

Koh SD, Jun JY, Kim TW, Sanders KM (2002) A Ca^{2+}-inhibited non-selective cation conductance contributes to pacemaker currents in mouse interstitial cell of Cajal. J Physiol 540:803–814

Mayer ML (1985) A calcium-activated chloride current generates the after-depolarization of rat sensory neurones in culture. J Physiol 364:217–239

Seul M, O'Gorman L, Sammon MJ (2000) Practical algorithms for image analysis: description, examples and code. Cambridge University Press, Cambridge

Sun XP, Supplisson S, Mayer E (1993) Chloride channels in myocytes from rabbit colon are regulated by a pertussis toxin sensitive G protein. Am J Physiol 264:G774–G785

Sun XP, Supplisson S, Torres R, Sachs G, Mayer E (1992) Characterization of large conductance chloride channels in rabbit colonic smooth muscle. J Physiol 448:355–382

Zhu Y, Mucci A, Huizinga JD (2005) Inwardly rectifying chloride channel activity in intestinal pacemaker cells. Am J Physiol 288:G809–G821